Environ. Water Eng., 2025, 11(3), 261-272 https://doi.org/10.22034/ewe.2025.487228.1980

EWE

Environment and Water Engineering

Homepage: www.jewe.ir

ISSN: 2476-3683

Investigation and comparison of carbon dioxide adsorption and fluidity behavior of activated carbon and titanium oxyhydroxide adsorbents

Masoumeh Lotfinezhad[1], and Maryam Tahmasebpoor[1]✉

[1]Department of Chemical & Petroleum Engineering, Faculty of Chemical & Petroleum Engineering, University of Tabriz, Tabriz, Iran

ARTICLE INFO

Paper Type: Research Paper

Received: 06 November 2024
Revised: 20 December 2024
Accepted: 04 January 2025
Published: 11 January 2025

Keywords
Fluidization
Fluidized Bed
Jujube Seeds
Nanoparticles
Silica

***Corresponding author:**
M. Lotfinezhad
✉ tahmasebpoor@tabrizu.ac.ir

ABSTRACT

This study examined and compared the adsorption behavior and fluidity of two common adsorbents: activated carbon made from jujube seeds and titanium oxyhydroxide (TiO(OH)2) used in carbon dioxide capture. The activated carbon was produced through chemical activation with potassium hydroxide as the activating agent at a 2:1 weight ratio to the biomass. To assess the characteristics of the adsorbents, techniques such as SEM, BET, FTIR, and TGA were employed. The carbon dioxide adsorption capacity was tested at 25 and 50 °C. Regeneration was performed at 120 °C with a gas flow rate of 50 cm^3/min. Adsorption was conducted for 1 hour, and desorption for 30 minutes, using 10% and 90% carbon dioxide concentrations in equilibrium with nitrogen. Results indicated that activated carbon had a significantly higher carbon dioxide adsorption capacity than $TiO(OH)_2$ under the same conditions. To evaluate the fluidity of the different adsorbents, a gas-solid fluidized bed apparatus was used. Adding 5% by weight of hydrophobic silica nanoparticles to the adsorbents improved fluidity and increased bed expansion, due to reduced cohesive interactions between particles. The comparison of results highlights the considerable effectiveness of activated carbon as an efficient adsorbent for carbon dioxide capture.

Highlights

- Jujube-seed carbon shows superior CO_2 adsorption vs. $TiO(OH)_2$.
- Microporous CJS enables higher capacity under mild conditions.
- SiO_2 nanoparticles improve adsorbent fluidization and bed expansion.

Citing:
Roushangar, K., Saadatjoo, R., Abbaszadeh, H., & Panahi, A. (2025). Prediction of air concentration in stepped spillways using data-oriented methods. *Environment and Water Eng*ineering, *11*(3), 261-272. https://doi.org/10.22034/ewe.2025.487228.1980

1. Introduction

The rising levels of CO_2 emissions in the atmosphere have garnered significant attention due to their correlation with climate change (Heidari et al., 2021). Currently, post-combustion carbon dioxide capture technologies encompass solvent absorption, adsorption, cryogenic methods, and membrane separation techniques (Heidari et al., 2023). Among these approaches, the use of solid adsorbents has garnered significant attention from researchers due to their advantages, including low corrosion rates, ease of operation, cost-effectiveness, reduced energy requirements, and high carbon dioxide adsorption capacity (Heidari et al., 2024). Activated carbon (AC) is regarded as a highly effective solid adsorbent due to its exceptional thermal and chemical stability, extensive porosity and surface area, cost efficiency, and reusability over multiple cycles (Liu et al., 2020). In their study, Toprak et al., (2017) investigated the CO_2 adsorption performance of AC adsorbents treated with various activating agents, including NaOH, KOH, and $ZnCl_2$. The highest CO_2 adsorption capacities recorded were 9.09 and 8.25 mmol/g, achieved under different activation conditions using KOH and NaOH at a temperature of 800 °C with a 4:1 ratio. Similarly, Athari et al., (2023) examined the CO_2 adsorption capabilities of AC derived from oleaster seeds. This research employed various activating agents such as KOH and $ZnCl_2$ at different ratios of 2:1, 3:1, and 4:1 to ascertain the impact of these ratios on CO_2 adsorption behavior. The findings indicated that KOH outperformed $ZnCl_2$ as an activating agent for CO_2 adsorption. Among the various activating agent to biomass ratios tested, the samples activated with KOH and $ZnCl_2$ at a 2:1 weight

ratio exhibited the highest average adsorption capacities of 2.78 and 1.74 mmol/g, respectively. Tahmasebpoor et al., (2023) focused on analyzing the CO_2 adsorption behavior of AC derived from waste tea. This study specifically explored the influence of two activating agents, KOH and NaOH, on the CO_2 adsorption capacity of the carbon adsorbent. The results revealed that the sample activated with KOH at a 1:1 ratio and a temperature of 600 °C demonstrated the highest CO_2 adsorption capacity, averaging 2.32 mmol/g at 25 °C and a CO_2 concentration of 90 vol%. Despite numerous studies on CO_2 adsorption using AC adsorbents, there is limited information regarding the capacity to adsorb other substances. One such substance is titanium oxyhydroxide ($TiO(OH)_2$), which is recognized for its catalytic properties and plays a significant role in the chemical absorption and removal of CO_2 in liquid systems, such as amine solutions (MEA), potassium bicarbonate ($KHCO_3$) solutions, and sodium bicarbonate ($NaHCO_3$) solutions. Given the efficacy of $TiO(OH)_2$ in CO_2 capture and disposal processes within liquid systems, there have also been limited investigations into its CO_2 adsorption capabilities in gas-solid systems. Tuwati et al. (2013) explored CO_2 adsorption using a synthesized $TiO(OH)_2$ adsorbent in conjunction with K_2CO_3. In this study, $TiO(OH)_2$ served as a base for K_2CO_3, resulting in a remarkable 37-fold increase in CO_2 adsorption capacity. The maximum CO_2 adsorption capacity achieved by this adsorbent was recorded at 1.69 mmol/g.

In numerous industrial adsorption processes, one critical parameter influencing the overall efficiency of solid adsorbents is their fluidization behavior. The examination of adsorbent fluidity is essential because if these materials exhibit poor fluidization characteristics, they can obstruct the expansion and flow of the bed during gas passage, thereby hindering effective contact between the gas phase and the solid phase (Iranvandi et al., 2023). Azimi et al., (2019) investigated the fluidization behavior of calcium oxide modified with aluminum. This research employed three types of additives, including hydrophilic silica nanoparticles, hydrophobic silica nanoparticles, and hydrophilic alumina, to coat the particles. The results indicated that hydrophobic silica nanoparticles significantly enhanced the fluidization behavior of the modified adsorbent.

Despite extensive studies conducted in this area, most research has shown that AC adsorbents derived from biomass waste possess a high capacity for carbon dioxide adsorption, with KOH activation positively impacting their adsorption performance. However, insufficient attention has been given to the development of highly fluidized AC adsorbents extracted from biomass for carbon dioxide capture processes. Furthermore, the CO_2 adsorption performance of $TiO(OH)_2$ adsorbents in gas-phase systems and environmental conditions has rarely been explored. On another note, the fluidity quality of both AC and $TiO(OH)_2$ adsorbents is a key parameter for the industrial application of CO_2 adsorbents in fluidized beds, yet it remains poorly understood.

The present study investigates the adsorption behavior and fluidization characteristics of AC derived from jujube seeds and $TiO(OH)_2$ adsorbents. This research represents a pioneering effort to compare and analyze both the adsorption and fluidization behaviors of these two adsorbents, underscoring its significant importance. Not only will this study lead to a deeper understanding of the adsorption and fluidization behaviors of the materials in question, but it may also provide strategies to enhance their performance in industrial and environmental applications.

2. Materials and Methods

2.1 Raw materials

The primary materials utilized in this research for the production of carbon-based adsorbents included jujube seed biomass sourced from the Iranian market, while titanium isopropoxide, purchased from Merck, served as the precursor for the $TiO(OH)_2$ adsorbent. Potassium hydroxide (KOH) from Merck, hydrochloric acid (HCl), and distilled water from Arman Sina, along with hydrophobic silica nanoparticles (Aerosil R972) obtained from Evonik, characterized by an initial particle size of 16 nm and a particle density of 2100 kg/m³, as well as a bulk density of 50 kg/m³, were also employed in this study.

2.2 Preparation of AC adsorbent

Initially, the jujube seed biomass was washed using distilled water. Subsequently, the washed seeds were dried in an oven at 100 °C for 24 hours. The biomass underwent carbonization in an air atmosphere at 600 °C for 2 hours, after which it was crushed and sieved through a 250 µm mesh. For the activation of the pyrolyzed biomass, KOH was used as an activating agent in a mass ratio of 2:1 relative to the biomass. Accordingly, 5 g of the pyrolyzed material was mixed with 10 g of the activating agent and stirred for 3 hours at 90 °C using a magnetic stirrer. To eliminate any remaining moisture, the resulting solution was placed in an oven at 90 °C for 24 hours. Following this step, the solid product obtained was subjected to a further activation process in a furnace at 600 °C for 1 hour. Upon completion of the activation process, the resulting sample was washed with a 3 M HCl solution and distilled water to remove excess potassium ions and neutralize it. Ultimately, the AC derived from jujube seeds was obtained by drying in an oven at 100 °C for 24 hours, followed by crushing and sieving through a 200 µm mesh (Shakeri et al., 2024). In this study, the pyrolyzed jujube seed and AC were designated as JS and CJS, respectively.

2.3 Preparation of $TiO(OH)_2$ adsorbent

To prepare the $TiO(OH)_2$ adsorbent, a specific amount of titanium isopropoxide was initially added to deionized water in a molar ratio of 1:1400. The resulting mixture was then stirred using a mechanical stirrer at room temperature for 4 hours to allow for precipitation, which was subsequently filtered. Finally, the obtained precipitate underwent three wash cycles with deionized water and ethanol using a centrifuge. The final adsorbent was dried in an oven at 100 °C for 10 hours (Asgharizadeh et al., 2023).

2.4 Physical mixing of adsorbents with hydrophobic SiO_2 nanoparticles

The AC adsorbents derived from JS, along with the $TiO(OH)_2$ adsorbent, were physically mixed with hydrophobic SiO_2 nanoparticles to assess their performance in enhancing fluidity behavior. For this purpose, the hydrophobic SiO_2 nanoparticles were manually mixed into the aforementioned samples at

weight percentages of 2.5% and 5% for a duration of 30 minutes. It is noteworthy that prior to mixing, the hydrophobic silica nanoparticles were sieved through a 150 µm mesh to eliminate any potential agglomerates (Imani et al., 2023).

2.5 Characterization

To investigate the morphology and structural characteristics of the synthesized adsorbents, scanning electron microscopy (SEM) analysis was conducted using a HOEL 6301F instrument. The specific surface area and pore volume were determined through Brunauer-Emmett-Teller (BET) analysis performed with a Tristar II 3020, where nitrogen isotherms were measured at -196 °C. Additionally, Fourier-transform infrared (FTIR) spectroscopy was utilized with a TENSOR 27 FTIR device to identify and characterize the compounds and functional groups present on the adsorbents. To assess the carbon dioxide adsorption capacity of the adsorbents over multiple cycles, thermogravimetric analysis (TGA) was carried out using equipment from INCAR-CSIC in Oviedo, Spain. TGA is a thermal analysis technique that monitors changes in the mass of the adsorbent as a function of temperature over time. Prior to testing, the adsorbent was heated to 120 °C in a nitrogen atmosphere to remove any initial moisture and adsorbed gases. The carbon dioxide adsorption capacity of the samples was evaluated at temperatures of 25 °C and 50 °C, with a regeneration temperature set at 120 °C. The experimental conditions included a gas flow rate of 50 cm^3/min, an adsorption duration of 1 hour, and a desorption period of 30 minutes, using carbon dioxide concentrations of 10% and 90% in equilibrium with nitrogen throughout successive cycles. The carbon dioxide uptake capacity (mmol/g) of the synthesized adsorbents was calculated by determining weight changes observed during the TGA tests, as described in Eq. 1 (Lotfinezhad et al., 2024a).

$$CO_2 \text{ uptake capacity} = \frac{M_n - M_0}{0.044 \times M_0} \quad (1)$$

In Eq. 1, M_n denotes the mass of the sample after n carbonation cycles, while M_0 represents the initial mass of the sample before the first cycle commenced. To evaluate the fluidization performance of the various adsorbents, a gas-solid fluidized bed apparatus was employed (Fig. 1). This system consists of a glass column with an internal diameter of 2.6 cm and a height of 80 cm, operated at ambient temperature and atmospheric pressure. Fluidization of the adsorbents was achieved using pure carbon dioxide, which was introduced into the bed through a distributor plate. To prevent the escape of fine particles at high velocities, a cyclone and air filter were installed above the column. The fluidization behavior of the particles was characterized using parameters such as bed expansion ratio (H/H_0) and pressure drop (Δp), where H_0 represents the initial bed height prior to carbon dioxide introduction and H indicates the bed height at a specified gas velocity. The pressure difference (Δp) between the two ends of the bed was measured using a manometer (WIKA pressure gauge) positioned between the top of the column and the distributor plate. All experiments were repeated three times with a 5-minute interval to enhance result accuracy and maintain stability conditions.

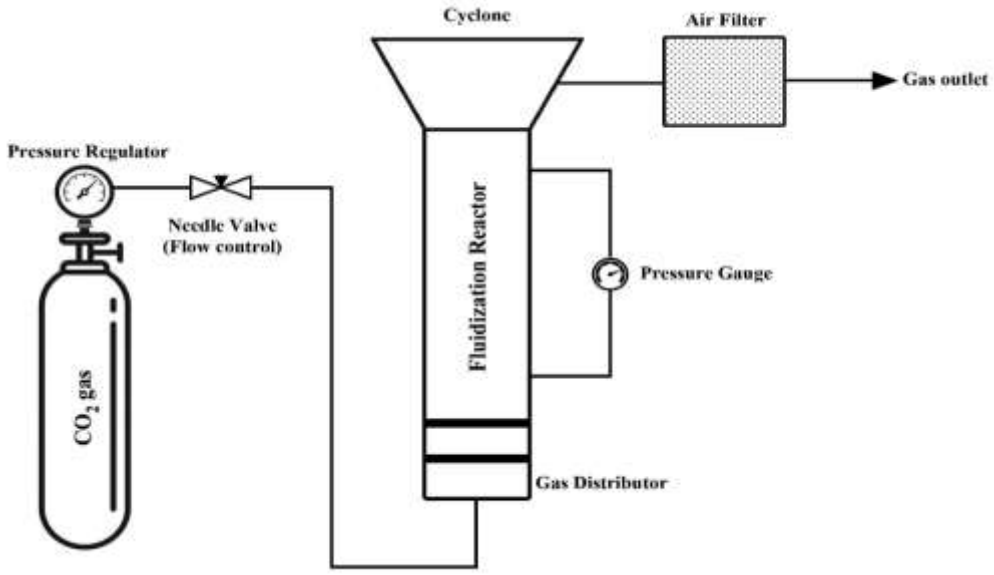

Fig. 1 Fluidized bed reactor schematic

3. Results and Discussion

3.1 Textural properties

Fig. 2 presents the morphological images obtained from the SEM analysis of JS, CJS, and $TiO(OH)_2$. As observed, the initial sample (JS) exhibits a smooth surface with limited microporosity (Fig. 2a). In contrast, the KOH-activated sample (Fig. 2b) displays a porous and cavernous structure, indicating the effectiveness of the KOH activation method in producing porous AC. The application of KOH as an efficient activating agent facilitates the formation and expansion of surface micropores, thereby enhancing the diffusion pathways for carbon dioxide molecule adsorption (Zhao et al., 2024). Three primary mechanisms of KOH activation are widely recognized: (a) the creation of carbon framework porosity through redox reactions between various potassium compounds and carbon; (b) the generation of H_2O and CO_2,

which positively contributes to further pore development via carbon gasification; and (c) the infiltration of metallic potassium into the carbon matrix, resulting in the expansion of carbon networks. The results depicted in Fig. 2c for $TiO(OH)_2$ indicate that its particles possess lower porosity compared to the AC sample, which likely hinders adequate carbon dioxide penetration into the $TiO(OH)_2$ adsorbent.

Fig. 2 SEM analysis images of a) JS, b) CJS and c) $TiO(OH)_2$ samples

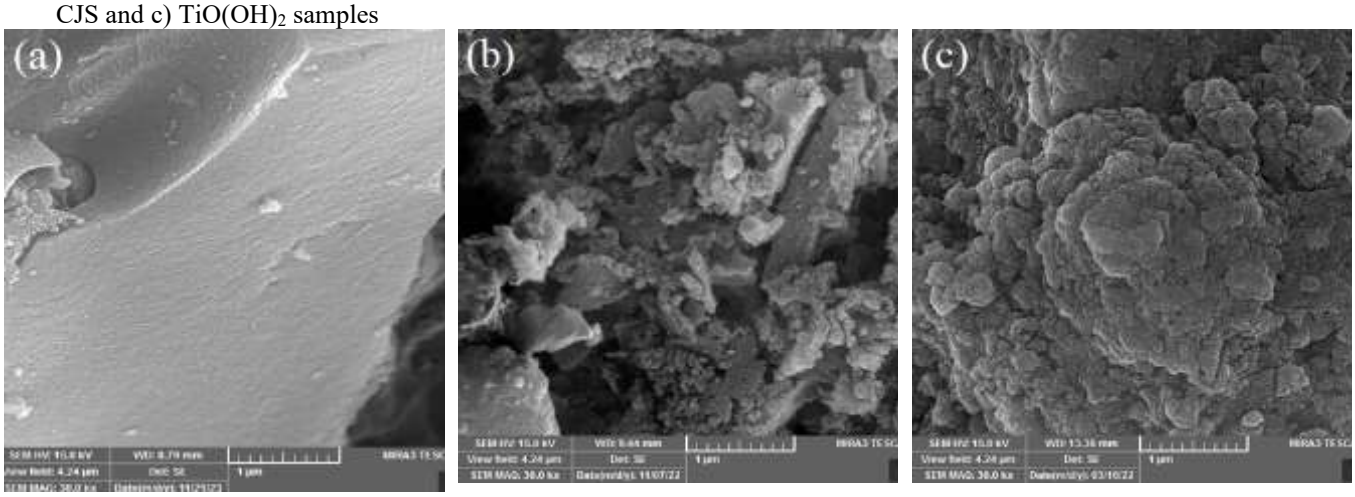

Fig. 3 illustrates the N_2 adsorption/desorption isotherm for the CJS sample at -196 °C. It is evident that the N_2 adsorption branch nearly overlaps with the desorption branch. As the relative pressure (P/P_0) increases up to 0.1, the adsorption curve reaches a horizontal plateau, which, according to IUPAC classification, signifies a Type I isotherm indicative of micropore presence. Furthermore, at relative pressures below 0.1, the CJS adsorbent demonstrates a significant increase in adsorption, suggesting that its structure predominantly consists of micropores. This adsorbent features a specific surface area of 698 m^2/g, a micropore volume of 0.26 cm^3/g, and a total pore volume of 0.32 cm^3/g.

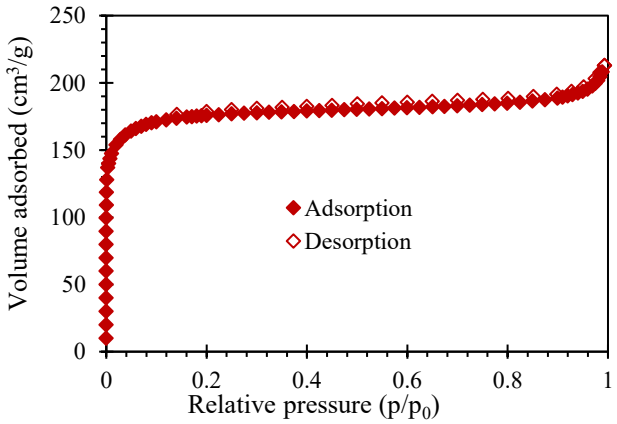

Fig. 3 N_2 adsorption/desorption isotherm of CJS sample at -196 °C

The FTIR spectra of the adsorbents JS, CJS, and $TiO(OH)_2$ are presented in Fig. 4 to confirm the presence of functional groups on their surfaces. For the biomass JS, relatively weak peaks are observed in the range of 3700 to 3900 cm^{-1}, which correspond to the stretching vibrations of OH groups due to moisture (Manyà et al., 2018). Additionally, a broad band between 3200 and 3600 cm^{-1} is attributed to hydroxyl groups (OH) from alcohols, phenols, and carboxylic acids. The presence of a peak at 1719 cm^{-1} indicates the existence of carboxyl and carbonyl bonds, both of which are considered oxygen-containing functional groups. On the surface of the raw biomass, aliphatic C-H stretching results in two distinct peaks at 2853 cm^{-1} and 2922 cm^{-1} (Serafin et al., 2021). Furthermore, a peak in the region of 1563 cm^{-1} signifies a C=O bond, while a distinct peak at 1874 cm^{-1} represents C-H bonds (de Salazar Martínez et al., 2024). Broad peaks in the range of 3000 to 3900 cm^{-1} in CJS are identified due to OH bonds arising from functional groups and absorbed moisture. Two weak peaks at 2853 cm^{-1} and 2923 cm^{-1} may be associated with aliphatic C-H bonds related to methyl and methylene groups (Liu et al., 2023). Additionally, other peaks observed in the KOH-modified sample at 1546 cm^{-1} are linked to C=O bonds such as carbonyl (Farshchi et al., 2024). The presence of C-O bonds in functional groups such as alcohols, carboxylic acids, ethers, and esters in the KOH-modified sample is indicated by broad peaks in the range of 900 to 1300 cm^{-1} (Zhu et al., 2024). In terms of functional groups on the surface of the adsorbent, the unactivated JS sample is richer compared to the activated sample, displaying more peaks. This can be attributed to the high-temperature activation process that leads to the decomposition of certain volatile materials in the sample and the removal of peaks present in the initial sample.

For the $TiO(OH)_2$ adsorbent, as observed, the peak at 3388 cm^{-1} corresponds to O-H stretching vibrations, indicating the presence of hydroxyl groups on the surface of the adsorbent (Zhou et al., 2024). Additionally, the peak observed at 1625 cm^{-1} is attributed to H-O-H vibrations from hydroxyl groups (Jin et al., 2023). Furthermore, a strong peak at 1112 cm^{-1} relates to Ti-O-C stretching (Song et al., 2024). Peaks at 1736 cm^{-1} and 640 cm^{-1} correspondingly indicate non-bonding TiO_2 and bending Ti-O vibrations, confirming the presence of Ti-O bonds (Lotfinezhad et al., 2024b).

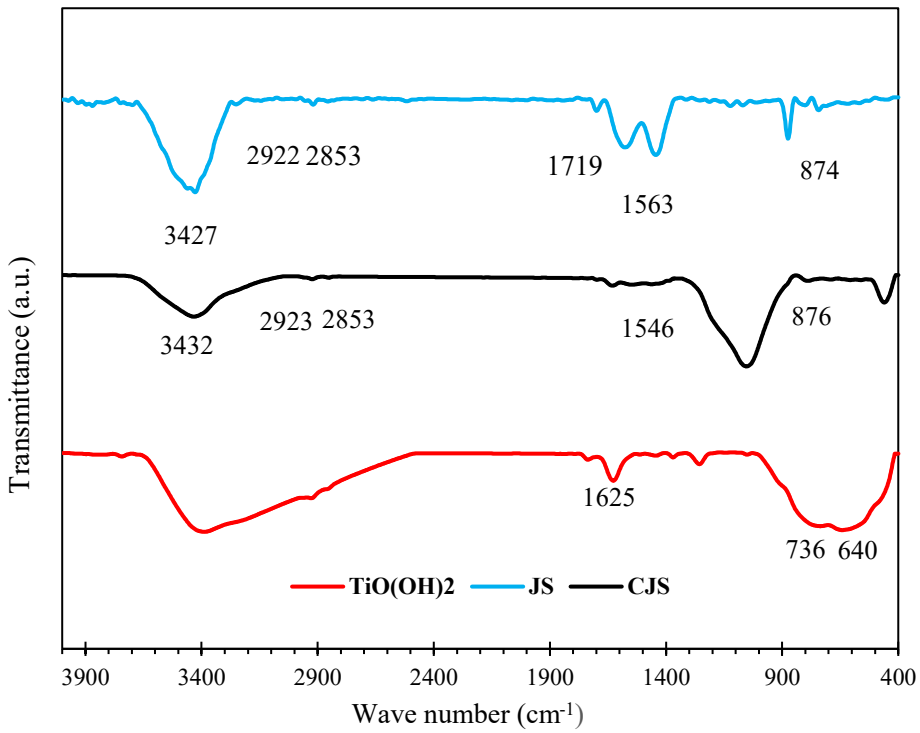

Fig. 4 FTIR analysis of JS, CJS, and $TiO(OH)_2$ samples

3.2 Performance of carbon dioxide adsorption by adsorbents

The adsorption performance of the CJS and $TiO(OH)_2$ samples was evaluated at temperatures of 25 °C and 50 °C, along with varying volumetric percentages of carbon dioxide (10% and 90%) mixed with nitrogen, across three consecutive cycles of adsorption and desorption to determine optimal adsorption conditions. Initially, the samples were subjected to a nitrogen gas flow at 120 °C to eliminate any potentially adsorbed gases (particularly carbon dioxide) and initial moisture. Following this, the temperature was lowered to the desired level, and the gas input was switched from pure nitrogen to a mixture of carbon dioxide and nitrogen, initiating the carbon dioxide adsorption process. The graphs depicting the amount of carbon dioxide adsorbed over time were generated. The TGA curves for the synthesized samples at 25 °C and 50 °C are illustrated in Fig. 5a and 5b. It is evident that the initial heating effectively removes moisture and adsorbed gases, resulting in a reduction in the weight of the samples. During the adsorption phase, when the samples are exposed to carbon dioxide gas, the overall mass of the adsorbents significantly increases due to the uptake and retention of carbon dioxide molecules. Conversely, during the desorption process, the adsorbed carbon dioxide molecules are released and separated.

Table 1 presents the average values of carbon dioxide adsorption by the CJS and $TiO(OH)_2$ adsorbents over three consecutive cycles of adsorption and desorption. As observed, an increase in temperature from 25 °C to 50 °C leads to a decrease in carbon dioxide adsorption affinity. For instance, as the temperature rises, the carbon dioxide adsorption capacities for the CJS and $TiO(OH)_2$ samples at a 10% volumetric concentration decrease from 1.16 mmol/g and 0.44 mmol/g to 0.67 mmol/g and 0.27 mmol/g, respectively. This reduction is attributed to the exothermic nature of the carbon dioxide adsorption process on these adsorbents. Consequently, higher temperatures result in diminished carbon dioxide adsorption capacities for both adsorbents under investigation. Additionally, as expected, an increase in carbon dioxide concentration in the incoming stream enhances its adsorption. For example, when the concentration of carbon dioxide rises from 10% to 90% volumetric, the carbon dioxide adsorption capacities for the CJS and $TiO(OH)_2$ samples at 25 °C reach 2.31 mmol/g and 0.77 mmol/g, respectively. The increased concentration of carbon dioxide in the gas stream improves its adsorption by enhancing interactions between carbon dioxide molecules and the adsorbent sites.

Based on TGA analysis results, it is evident that the adsorption capacity of CJS and $TiO(OH)_2$ adsorbents decreases with increasing temperature while increasing with higher carbon dioxide concentrations. For instance, the average carbon dioxide adsorption for CJS at a 90% volumetric concentration reaches 2.31 mmol/g, which is approximately 1.54 mmol/g higher than that of $TiO(OH)_2$ at 0.77 mmol/g. A comparison of the adsorption results and SEM images indicates that AC adsorbents exhibit superior performance compared to $TiO(OH)_2$ due to their developed pore structure. Previous studies have demonstrated that $TiO(OH)_2$ forms strong hydrogen bonds and interparticle forces such as van der Waals interactions due to its polar structure and the presence of O and H atoms. These predominant internal forces lead to particle agglomeration, consequently significantly diminishing the carbon dioxide adsorption performance of this adsorbent.

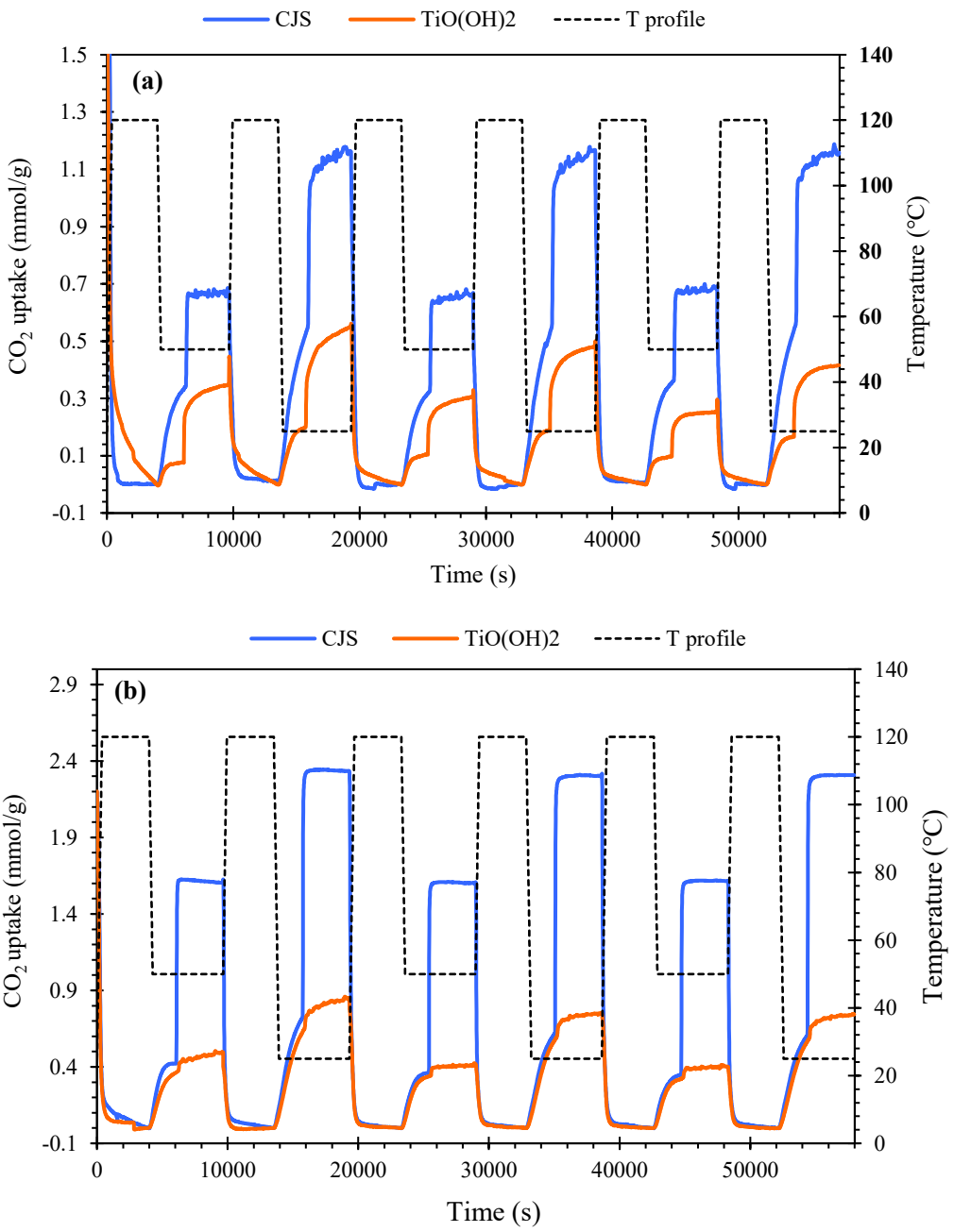

Fig. 5 TGA profile of CJS and $TiO(OH)_2$ adsorbents at different adsorption temperatures of 25 °C and 50 °C and desorption temperature of 120 °C in the presence of a)10 and b) 90 vol% CO_2

Table 1 CO_2 adsorption capacities of CJS and $TiO(OH)_2$ at adsorption temperatures of desorption temperature of 120 °C, N_2 balance (average three cycles)

Sample	CO_2 uptake capacity unit	Average CO_2 uptake (10 vol% CO_2)		Average CO_2 uptake (90 vol% CO_2)	
		T= 25 °C	T= 50 °C	T= 25 °C	T= 50 °C
CJS	wt%	5.09	2.96	10.18	7.06
	mmol/g	1.16	0.67	2.31	1.60
$TiO(OH)_2$	wt%	1.97	1.22	3.28	1.79
	mmol/g	0.44	0.27	0.77	0.4

A review of recent studies on ACs derived from various biomass residues for carbon dioxide adsorption is presented in Table 2. This comparison indicates that the AC developed in this research is among the most efficient and robust adsorbents

for carbon dioxide in terms of adsorption capacity. It is also noteworthy that this adsorbent is produced from waste materials that are widely available in Asia, making it more suitable from both economic and ease of production perspectives. On the other hand, catalytic carbon dioxide adsorption has emerged as a crucial component in carbon capture and storage (CCS) technology in recent years. $TiO(OH)_2$ has been investigated in several recent studies as an effective catalytic adsorbent for carbon dioxide. The $TiO(OH)_2$ synthesized in this study demonstrated favorable results for carbon dioxide adsorption at 25 °C and 1 bar pressure.

Table 2 The performance of ACs derived from biomass residues using chemical activation in the process of carbon dioxide adsorption

Precursor	Activating agent	Adsorption Temperature (°C)	CO_2 concentration (vol%)	CO_2 uptake (mmol/g)	Ref.
Date seed	KOH	25	15	1.19	Iranvandi et al. (2023)
Jujun grass	KOH	25	15	0.90	Coromina et al. (2016)
Phenolic resin	HNO_3	30	15	0.91	Sun et al. (2015)
Black locust	KOH	25	15	0.75	Zhang et al. (2016)
Jujube seeds	KOH	25	10	1.16	This study
Jujube seeds	KOH	25	90	2.43	This study

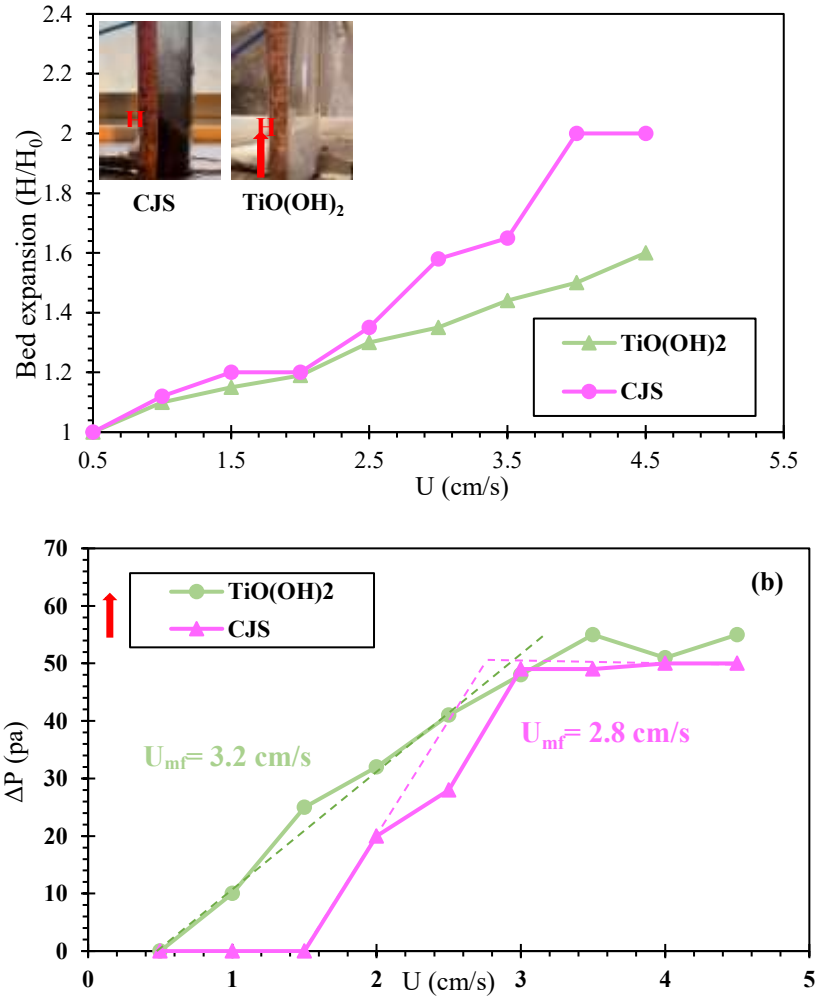

Fig. 6 a) bed expansion curves and b) pressure drop curves for CJS and $TiO(OH)_2$ samples

3.3 Performance fluidity of AC and $TiO(OH)_2$ adsorbents

For effective utilization of adsorbents in industrial processes, it is essential not only to have a high adsorption capacity but also to ensure adequate dispersion of these materials. In this study, the fluidity behavior of the CJS and $TiO(OH)_2$ adsorbents was examined before and after the addition of hydrophobic silica nanoparticles at weight percentages of 2.5% and 5% in a low-speed laboratory fluidized bed ranging from 0.5 to 4.5 cm/s. The bed expansion values and pressure drop profiles for the CJS and $TiO(OH)_2$ samples are illustrated in Fig. 6a and 6b. The results indicate that the bed expansion ratio for CJS and $TiO(OH)_2$ reached 2 and 1.6, respectively, at a gas velocity of 4.5 cm/s. Another important parameter to consider for calculating U_{mf} is the change in bed pressure drop with increasing velocity, which was reported to be

approximately 2.8 cm/s and 3.2 cm/s for these particles, respectively. It is important to note that adhesive forces between particles hinder complete bed expansion at velocities exceeding U_{mf}, resulting in heterogeneous fluidity behavior. Visual observations also confirm the presence of large agglomerates, a bubbly regime, and stable gas channels. Consequently, in this study, the low bed expansion values, high U_{mf}, and heterogeneous fluidity behavior accompanied by the formation of channels, bubbles, and large agglomerates are recognized as ABF fluidity behavior. Therefore, there is a pressing need to develop methods to enhance the fluidity quality of these samples to improve their carbon dioxide adsorption capabilities.

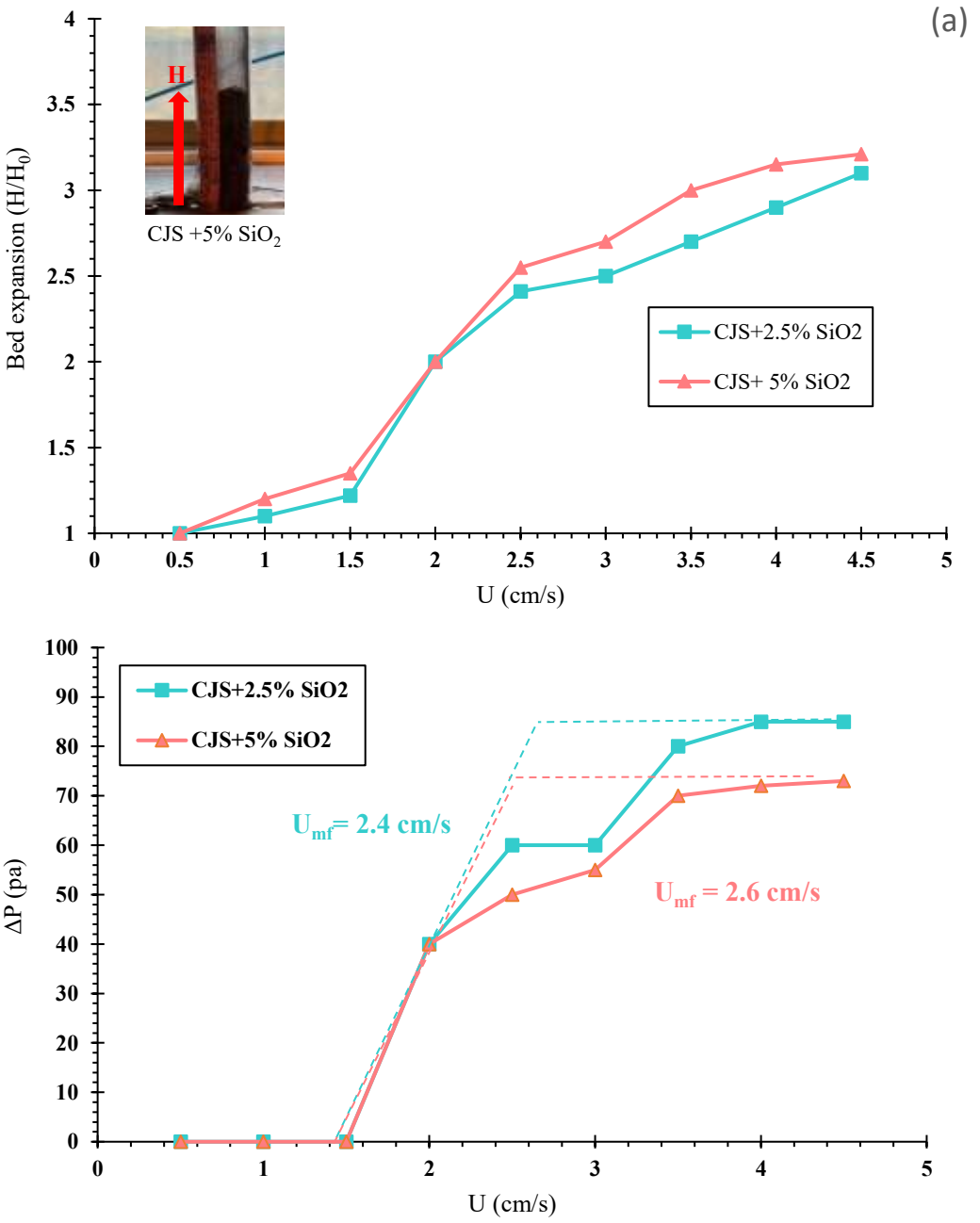

Fig. 7 a) bed expansion curves and b) pressure drops curves for binary mixtures of (CJS+SiO_2) in the presence of 2.5 and 5 wt% SiO_2

3.4 Fluidity performance of binary mixtures of AC and SiO_2

Figure 7a and 7b illustrate the bed expansion ratio and pressure drop curves for the binary mixture of CJS and SiO_2 at weight percentages of 2.5% and 5%. As depicted in Fig. 7a, the incorporation of SiO_2 nanoparticles into the CJS bed significantly enhances the bed expansion ratio, thereby improving fluidity performance. The SiO_2 nanoparticles not only diminish the van der Waals forces between the adsorbent particles but also exhibit favorable fluidity behavior. Consequently, these nanoparticles disperse among the adsorbent particles, contributing to an overall enhancement of the bed properties. For instance, at a gas velocity of 4.5 cm/s, the bed expansion ratios for the CJS mixtures with 2.5% and 5% SiO_2 reach approximately 3.1 and 3.21, respectively. At lower velocities, the expansion for the SiO_2-modified samples

is reduced, which can be attributed to channel formation. However, as the concentration of SiO_2 nanoparticles increases, the number of channels decreases, with no channels observed at velocities exceeding 3 cm/s. Additionally, the introduction of this easily fluidizable material into the pure adsorbent bed eliminates surface fluctuations. The U_{mf} values obtained from the pressure drop curves for CJS in the presence of 2.5% and 5% SiO_2 indicate that fluidization begins at 2.6 cm/s and 2.4 cm/s, respectively (Fig. 7b). This trend demonstrates that an increase in the weight percentage of silica results in a reduction in U_{mf}.

3.5 Fluidity performance of binary mixtures of $TiO(OH)_2$ and SiO_2

To enhance the fluidization performance of $TiO(OH)_2$ adsorbent, varying weight percentages of hydrophobic SiO_2 nanoparticles, specifically 2.5% and 5%, were incorporated into the adsorbent. Figs. 8a and 8b present the bed expansion and pressure drop curves over a gas velocity range of 0.5 to 4.5 cm/s for the adsorbent. The addition of SiO_2 nanoparticles appears to exert a beneficial effect on the bed expansion ratio, thereby improving the fluidization quality of the adsorbent. The bed expansion ratios for the $TiO(OH)_2$ combined with SiO_2 at weight percentages of 2.5% and 5% reach values of 2.6 and 2.9, respectively. The increase in bed expansion from 1.6 to 2.6 and 2.9 confirms the positive influence of SiO_2 nanoparticles on the fluidization behavior of the adsorbent. Consequently, the homogeneous fluidity of the particles replaces severe channeling, resulting in a liquid-like behavior. It can be inferred that the optimal addition of SiO_2 nanoparticles as a carrier for the adsorbent particles leads to an enhancement of electrostatic forces at the contact points between the nanoparticles and the base adsorbent. A more uniform and extensive coating of the adsorbent particles with SiO_2 nanoparticles contributes to improved fluidity performance and effective gas-solid interaction. Furthermore, the U_{mf} values, at which the pressure drop between the two ends of the fluidized bed stabilizes, were determined to be 2.8 cm/s and 2.62 cm/s for $TiO(OH)_2$ combined with 2.5% and 5% SiO_2 by weight, respectively, further affirming the positive role of SiO_2 nanoparticles in enhancing the fluidization behavior of the adsorbent.

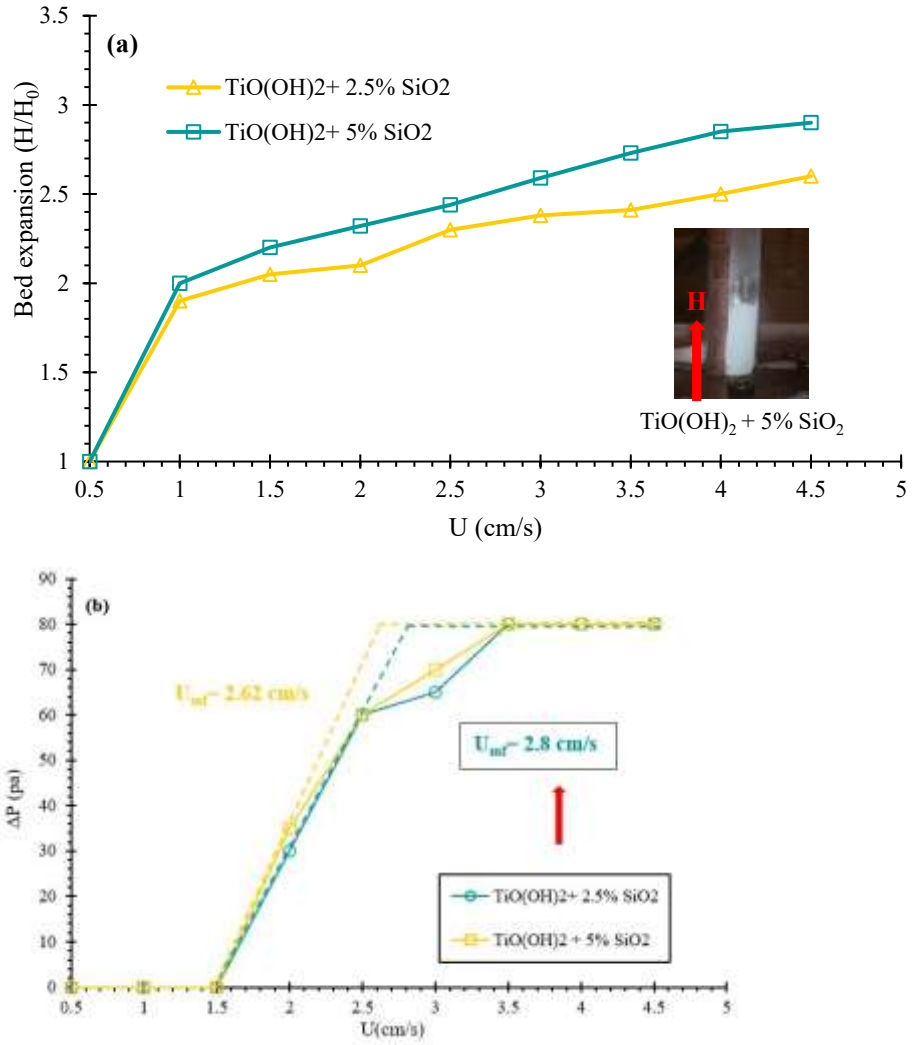

Fig. 8 a) Bed expansion curves and b) pressure drops curves for binary mixtures of ($TiO(OH)_2$ + SiO_2) in the presence of 2.5 and 5 wt% SiO_2

In industrial applications, fluidized beds are widely utilized to increase the contact surface area between solids and gases, consequently enhancing carbon dioxide adsorption capacity. This study has demonstrated that CJS exhibits effective fluidization performance. Additionally, it has been shown for the first time that the fluidization capability of synthesized $TiO(OH)_2$ has been improved in a dry gas environment.

4. Conclusion

In this study, AC derived from jujube seeds (CJS) was evaluated as an effective adsorbent for carbon dioxide, and its adsorption capacity and fluidization behavior were compared with those of the $TiO(OH)_2$ adsorbent. The results obtained indicated that:

1. The adsorption capacity of the CJS adsorbent, at 2.31 mmol/g under optimal conditions (25 °C and 90% volumetric concentration of carbon dioxide), was significantly higher than that of the $TiO(OH)_2$ adsorbent, which had a capacity of 0.77 mmol/g.

2. SEM images revealed that this difference in adsorption performance was clearly attributable to the developed microporous structure of CJS, which facilitates higher adsorption capabilities.

3. At a gas velocity of 4.5 cm/s, the bed expansion ratios for the adsorbents CJS and TiO(OH)2 mixed with 2.5% and 5% SiO2 nanoparticles were 3.1, 3.21, 2.6, and 2.9, respectively, significantly higher than without SiO2. However, the positive effect of SiO2 on the fluidization of TiO(OH)2 was limited due to strong interparticle adhesive forces, including van der Waals interactions and hydrogen bonding.

4. The incorporation of hydrophobic SiO_2 nanoparticles resulted in a remarkable enhancement in the fluidization performance of the adsorbents, demonstrating that an increase in the weight percentage of these additives significantly improved bed expansion and reduced U_{mf}.

Overall, the findings of this research not only affirm the superiority of the CJS sample in terms of carbon dioxide adsorption and fluidization performance but also suggest promising industrial applications for this adsorbent in pollution control processes and energy resource optimization. Nevertheless, additional necessary steps must be taken to address remaining challenges in future studies. For instance, it is recommended that adsorption/desorption cycles be conducted in a fluidized bed system under industry-relevant conditions rather than using TGA, as this approach would provide a more realistic and practical assessment of the performance of synthesized adsorbents. The separation and wear of particles in fluidized beds when subjected to real flow conditions present a challenge that requires attention. Enhancing the mechanical strength of adsorbents to reduce their wear in fluidized reactors is critically important. Given the limited performance of $TiO(OH)_2$ in gaseous environments compared to aqueous settings due to the polar characteristics of $TiO(OH)_2$ and the non-polar nature of carbon dioxide, conducting fluidization tests in the presence of moisture or hydrophilic alcohols that facilitate interactions between the adsorbent molecules could represent a significant step forward.

Statements and Declarations

Data Availability

The data generated in this research is presented in the text of the article.

Conflict of interest

The authors of this paper declared no conflict of interest regarding the authorship or publication of this article

Author contribution

M. Lotfinezhad: Writing – original draft, Methodology, Investigation, Conceptualization, and M. Tahmasebpoor: Writing –review & editing, Supervision.

AI Use Declaration

This study did not incorporate artificial intelligence techniques; instead, all analyses and optimizations were conducted using conventional and widely accepted analytical methods.

References

Asgharizadeh, K., Tahmasebpoor, M., Azimi, B., & Imani, M. (2024). Fluidity comparison of biomass-derived activated carbon and TiO $(OH)_2$ and its improving toward promoted low-temperature CO_2 capture in gaseous medium. *Chemical Engineering Research and Design, 202,* 23-37. DOI: https://doi.org/10.1016/j.cherd.2023.12.019.

Athari, M.-J., Tahmasebpoor, M., Azimi, B., Heidari, M., & Pevida, C. (2023). Waste oleaster seed-derived activated carbon mixed with coarse particles of fluid catalytic cracking as a highly-efficient CO_2 adsorbent at low temperatures. *Process Safety and Environmental Protection, 178,* 580-594. DOI: https://doi.org/10.1016/j.psep.2023.08.062.

Azimi, B., Tahmasebpoor, M., Sanchez-Jimenez, P. E., Perejon, A., & Valverde, J. M. (2019). Multicycle CO_2 capture activity and fluidizability of Al-based synthesized CaO sorbents. *Chemical Engineering Journal, 358,* 679-690. DOI: https://doi.org/10.1016/j.cej.2018.10.061.

de Salazar Martínez, E. M., Alexandre-Franco, M. F., Nieto-Sánchez, A. J., & Cuerda-Correa, E. M. (2024). Exploring the role of surface and porosity in CO2 capture by CaO-based adsorbents through response surface methodology (RSM) and artificial neural networks (ANN). *Journal of CO_2 Utilization, 83,* 102773. DOI: https://doi.org/10.1016/j.jcou.2024.102773.

Farshchi, M. E., Asgharizadeh, K., Jalili, H., Nejatbakhsh, S., Azimi, B., Aghdasinia, H., & Mohammadpourfard, M. (2024). Bimetallic MOF@ CdS nanorod composite for highly efficient piezo-photocatalytic CO_2 methanation under visible light. *Journal of Environmental Chemical Engineering, 12(5),* 113909. DOI: https://doi.org/10.1016/j.jece.2024.113909.

Heidari, M., Mousavi, S. B., Rahmani, F., Aminabhavi, T. M., & Rezakazemi, M. (2023). Insightful textural/morphological evaluation of cost-effective and highly sustainable Ca-Zr-O nanosorbent modified with the waste date kernel as a biomass pore-former for high-temperature CO2 capture. *Sustainable Materials and Technologies, 38,* e00778. DOI: https://doi.org/10.1016/j.susmat.2023.e00778.

Heidari, M., Mousavi, S. B., Rahmani, F., & Sene, R. A. (2024). Eco-friendly, sustainable and porous eggshell/tea

waste-derived CaO nanoparticles as a high-temperature CO_2 sorbent: Fabrication and textural/morphological evaluation. *Journal of Industrial and Engineering Chemistry, 134,* 169-180. DOI: https://doi.org/10.1016/j.jiec.2023.12.048.

Heidari, M., Tahmasebpoor, M., Antzaras, A., & Lemonidou, A. A. (2020). CO_2 capture and fluidity performance of CaO-based sorbents: Effect of Zr, Al and Ce additives in tri-, bi-and mono-metallic configurations. *Process Safety and Environmental Protection, 144,* 349-365. DOI: https://doi.org/10.1016/j.psep.2020.07.041.

Heidari, M., Tahmasebpoor, M., Mousavi, S. B., & Pevida, C. (2021). CO_2 capture activity of a novel CaO adsorbent stabilized with (ZrO_2+ Al_2O_3+ CeO_2)-based additive under mild and realistic calcium looping conditions. *Journal of CO_2 Utilization, 53,* 101747. DOI: https://doi.org/10.1016/j.jcou.2021.101747.

Imani, M., Tahmasebpoor, M., Sánchez-Jiménez, P.E., Valverde, J.M., & Moreno, V. (2023). A novel, green, cost-effective and fluidizable SiO_2-decorated calcium-based adsorbent recovered from eggshell waste for the CO_2 capture process. *Separation and Purification Technology, 305,* 122523. DOI: https://doi.org/10.1016/j.seppur.2022.122523.

Iranvandi, M., Tahmasebpoor, M., Azimi, B., Heidari, M., & Pevida, C. (2023). The novel SiO_2-decorated highly robust waste-derived activated carbon with homogeneous fluidity for the CO_2 capture process. *Separation and Purification Technology, 306,* 122625. DOI: https://doi.org/10.1016/j.seppur.2022.122625.

Jin, B., Wang, R., Fu, D., Ouyang, T., Fan, Y., Zhang, H., & Liang, Z. (2023). Chemical looping CO2 capture and in-situ conversion as a promising platform for green and low-carbon industry transition: Review and perspective. *Carbon Capture Science & Technology,* 100169. DOI: https://doi.org/10.1016/j.ccst.2023.100169.

Liu, G., Sun, S., Sun, H., Zhang, Y., Lv, J., Wang, Y., . .. & Wu, C. (2023). Integrated CO_2 capture and utilisation: A promising step contributing to carbon neutrality. *Carbon Capture Science & Technology, 7,* 100116. DOI: https://doi.org/10.1016/j.ccst.2023.100116.

Liu, J., Baeyens, J., Deng, Y., Tan, T., & Zhang, H. (2020). The chemical CO_2 capture by carbonation-decarbonation cycles. *Journal of Environmental Management, 260,* 110054. DOI: https://doi.org/10.1016/j.jenvman.2019.110054.

Lotfinezhad, M., Tahmasebpoor, M., & Pevida, C. (2024a). Exploring the structural characteristics and adsorption capabilities of cost-effective N-doped activated carbon derived from waste biomass for CO_2 adsorption. *Environmental Research,* 120017. DOI: https://doi.org/10.1016/j.envres.2024.120017.

Lotfinezhad, M., Tahmasebpoor, M., & Pevida, C. (2024b). The effect of humidity on the enhanced CO_2 adsorption of amine-functionalized microporous activated carbon. *Environmental Science and Pollution Research,* 1-14. DOI: https://doi.org/10.1007/s11356-024-35559-x.

Manyà, J. J., González, B., Azuara, M., & Arner, G. (2018). Ultra-microporous adsorbents prepared from vine shoots-derived biochar with high CO_2 uptake and CO_2/N_2 selectivity. *Chemical Engineering Journal, 345,* 631-639. DOI: https://doi.org/10.1016/j.cej.2018.01.092.

Serafin, J., Ouzzine, M., Junior, O. F. C., & Sreńscek-Nazzal, J. (2021). Preparation of low-cost activated carbons from amazonian nutshells for CO_2 storage. *Biomass and Bioenergy, 144,* 105925. DOI: https://doi.org/10.1016/j.biombioe.2020.105925.

Shahkarami, S., Azargohar, R., Dalai, A. K., & Soltan, J. (2015). Breakthrough CO_2 adsorption in bio-based activated carbons. *Journal of Environmental Science, 34,* 68-76. DOI: https://doi.org/10.1016/j.jes.2015.03.008.

Shakeri, N., Barzegar, B., Habibi, R., Aghdasinia, H., & Altinkaya, S. A. (2024). Enhanced performance and anti-fouling properties of polyether sulfone (PES) membranes modified with pistachio shell-derived activated carbon (PSAC)@ ZIF-8&ZIF-67 to remove dye contaminants. *International Journal of Biological Macromolecules,* 137654. DOI:https://doi.org/10.1016/j.ijbiomac.2024.137654

Song, C., Run, L., Liu, Q., Deng, S., Li, H., & Sun, J. (2024). Membrane-cryogenic hybrid CO_2 capture—A review. *Carbon Capture Science and Technology, 13,* 100249. DOI: https://doi.org/10.1016/j.ccst.2024.100249.

Sun, N., Sun, C., Liu, J., Liu, H., Snape, C. E., Li, K., Wei, W., & Sun, Y. (2015). Surface-modified spherical activated carbon materials for pre-combustion carbon dioxide capture. *RSC Advances, 5(42),* 33681-33690. DOI: https://doi.org/10.1039/C5RA02665B.

Tahmasebpoor, M., Iranvandi, M., Heidari, M., Azimi, B., & Pevida, C. (2023). Development of novel waste tea-derived activated carbon promoted with SiO_2 nanoparticles as highly robust and easily fluidizable sorbent for low-temperature CO_2 capture. *Journal of Environmental Chemical Engineering, 11(5),* 110437. DOI: https://doi.org/10.1016/j.jece.2023.110437.

Toprak, A., & Kopac, T. (2017). Carbon dioxide adsorption using high surface area activated carbons from local coals modified by KOH, NaOH and $ZnCl_2$ agents. *International Journal of Chemical Reactor Engineering, 15(3),* 20160042. DOI: https://doi.org/10.1515/ijcre-2016-0042.

Tuwati, A., Fan, M., Russell, A.G., Wang, J., & Dacosta, H.F. (2013). New CO_2 sorbent synthesized with nanoporous $TiO(OH)_2$ and K_2CO_3. *Energy & Fuels 27,* 7628-7636. DOI: https://doi.org/10.1021/ef401368n.

Zhang, C., Song, W., Ma, Q., Xie, L., Zhang, X., & Guo, H. (2016). Enhancement of CO_2 capture on biomass-based carbon from black locust by KOH activation and ammonia modification. *Energy & Fuels, 30(5),* 4181-4190. DOI: https://doi.org/10.1021/acs.energyfuels.5b02764.

Zhao, J., Zhang, W., Wang, Q., Shen, D., & Wang, Z. (2024). Lignin-derived porous carbons for efficient CO_2 adsorption. *Carbon Capture Science & Technology, 13,* 100233. DOI: https://doi.org/10.1016/j.ccst.2024.100233.

Zhou, X., Wang, D., Liu, C., Jing, G., Lv, B., & Wang, D. (2024). Enhancing CO_2 capture of an aminoethylethanolamine-based non-aqueous absorbent by using tertiary amine as a proton-transfer mediator: From performance to mechanism. *Journal of Environmental Science, 140,* 146-156. DOI: https://doi.org/10.1016/j.ccst.2024.100233.

Zhu, W., Wang, Y., Yao, F., Wang, X., Zheng, H., Ye, G., Cheng, H., Wu, J., Huang, H., & Ye, D. (2024). One-pot synthesis of N-doped petroleum coke-based microporous carbon for high-performance CO_2 adsorption and supercapacitors. *Journal of Environmental Science, 139,* 93-104. DOI: https://doi.org/10.1016/j.jes.2023.02.008.

© Authors, Published by *Environ. Water Eng*. Journal. This is an open-access article distributed under the CC BY (license http//creativecommons.org.licenses.by.4.0).